Alma Mater Studiorum
Università di Bologna

SCUOLA DI SCIENZE
Corso di Laurea in Fisica

Neutron radiation resistance of photomultipliers for the LUCID detector in the ATLAS experiment at LHC

Relatore:
Chiar.mo Prof.
Nicola Semprini-Cesari
Correlatore:
Dott.ssa Carla Sbarra

Presentata da:
Valentina Cicero

Sessione II
Anno Accademico 2014-2015

Abstract (English)

After a phase called Long Shutdown 1 (LS1), LHC restarted operations in May 2015, and is expected to reach doubled beam energy and instantaneous luminosity with respect to RUN 1 (2008-2012). Luminosity is an important parameter for a collider, as it correlates the event rate of any process to its cross section, and a precise measurement of it is necessary.
At the ATLAS experiment instantaneous and integrated luminosity are provided by, among others, a dedicated luminosity monitor: the LUCID detector. Before the LS1, LUCID consisted of two modules, each composed by 20 aluminum tubes filled with a Cherenkov gas and coupled with a photomultiplier (PMT) with a quartz window. Particles produced by pp interactions emit photons by Cherenkov effect when they cross the gas and the PMT window. This allowed LUCID to determine relative luminosity by counting hits (PMT signals above a given threshold).
The PMT ageing during the first phase of LHC operations, and the high luminosity expected for the second one, called for an upgrade of LUCID. In the new detector, some systematic effects that started to manifest during the years 2011-2012, namely the loss of linearity at the largest instantaneous luminosity and saturation of counting algorithms, will be minimized as well. As a replacement of PMTs was necessary anyway due to the total current sustained before LS1, it was decided to use a different PMT model, with a smaller acceptance, so as to reduce the hit rate.
Two PMT models were considered. One specimen per model was irradiated both with gammas and neutrons in order to look for possible variations of

its operational parameters due to the absorbed radiation. This thesis is dedicated to the study of effects induced by neutrons.

After an introduction to LHC and the ATLAS experiment (Chapter 1), a description of the methods used to measure luminosity at hadron colliders, and in ATLAS in particular, is provided in Chapter 2, together with a summary of LUCID performance during Phase I operations. Chapter 3 focuses on the principle of operation of photomultipliers and their main characteristics. In Chapter 4 the strategy used for measuring neutron radiation resistance, data analysis and final results are described.

Abstract (Italiano)

Dopo una fase di chiusura, detta Long Shutdown 1 (LS1), LHC ha ripreso le operazioni a maggio 2015 con energia dei fasci raddoppiata rispetto al RUN 1 (2008-2012). Ci si aspetta che anche la luminosità istantanea sarà presto raddoppiata. La luminosità è un parametro importante per un collider, in quanto mette in relazione la frequenza di eventi di ogni processo con la sua sezione d'urto, ed una sua misura precisa è necessaria.
Presso l'esperimento ATLAS la luminosità istantanea è fornita da diversi rivelatori, tra cui uno dedicato: il rivelatore LUCID. Prima del LS1, LUCID comprendeva due moduli, ognuno composto da 20 tubi di alluminio riempiti con un gas Cherenkov e accoppiati a un fotomoltiplicatore (PMT) con finestra di quarzo. Le particelle prodotte da un'interazione emettono fotoni per effetto Cherenkov quando attraversano il gas e la finestra di quarzo del PMT. Ciò ha permesso a LUCID di determinare la luminosità relativa contando le hit (segnali sopra una certa soglia).
L'invecchiamento dei PMT durante la prima fase di LHC e l'alta luminosità attesa dopo il LS1 hanno richiesto un aggiornamento di LUCID. Il nuovo rivelatore sarà anche in grado di minimizzare alcuni effetti sistematici che hanno iniziato a manifestarsi durante gli anni 2011-2012: la perdita di linearità alla massima luminosità istantanea e la saturazione di alcuni algoritmi di conteggio. Essendo comunque necessario sostituire i PMT, si è deciso di utilizzare un modello di PMT diverso, con un'accettanza minore, al fine di ridurre la frequenza delle hit e la corrente passante nelle catene dinodiche dei PMT.

Sono stati considerati due possibili modelli di PMT. Un esemplare per ogni modello è stato sottoposto a radiazione gamma e di neutroni per misurarne la resistenza a tali radiazioni. Questa tesi è in particolare dedicata allo studio della resistenza dei PMT alla radiazione di neutroni.

Dopo un'introduzione su LHC e sull'esperimento ATLAS (Capitolo 1), nel Capitolo 2 è fornita una descrizione dei metodi utilizzati per misurare la luminosità nei collisionatori adronici e, in particolare, in ATLAS, assieme a un'analisi delle prestazioni di LUCID negli anni 2010-2012. Il Capitolo 3 è incentrato sulla descrizione del funzionamento e delle principali caratteristiche dei fotomoltiplicatori. Infine, nel Capitolo 4 è descritta la strategia utilizzata per verificare la resistenza dei PMT alle radiazioni, sono forniti i risultati delle misure, la loro analisi e le conclusioni.

Contents

Chapter 1

The Large Hadron Collider

This chapter provides a brief introduction to the *Large Hadron Collider* (LHC) and the ATLAS detector at the CERN Laboratory nearby Geneva.

1.1 The Large Hadron Collider

The *Large Hadron Collider* (LHC) is the world's largest and most powerful particle accelerator [1]. The collider is contained in a circular tunnel with a circumference of 27 kilometres, formerly used to house the *Large Electron-Positron Collider* (LEP), at a depth ranging from 50 to 175 metres underground.
The LHC collides protons - and lead ions during one month per year - in four different points along the ring, corresponding to the location of four experiments:

- **ALICE** *(A Large Ion Collider Experiment)*: a detector specialized in analysing lead-ion collisions. It is designed to study the physics of quark-gluon plasma.

- **ATLAS** *(A Toroidal LHC ApparatuS)*: a general-purpose detector designed to cover the widest range of physics at LHC. Its structure will be showed in detail in Section 1.2.

- **CMS** *(Compact Muon Solenoid)*: a general-purpose detector with the same goals as ATLAS, but different technical solutions and design.
- **LHCb**: an experiment specialized on b-physics, and specially aimed at measuring the parameters of CP violation in the interactions of b-hadrons.

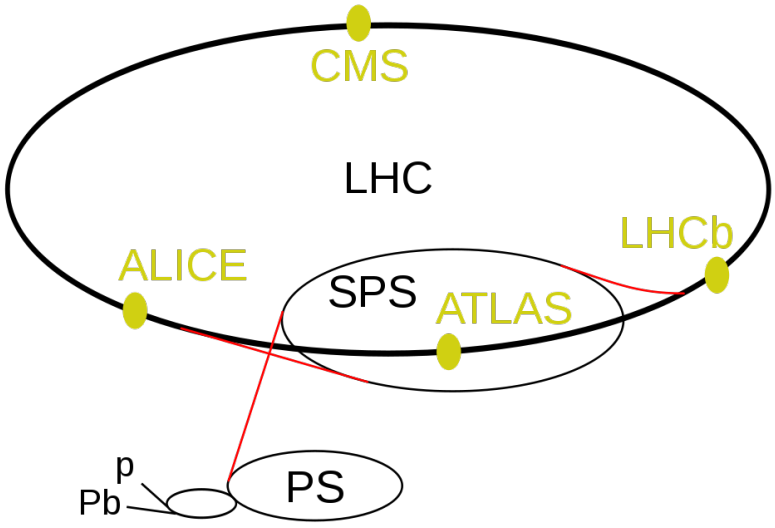

Figure 1.1: The LHC ring with the four experiments and the preaccelerators.

Fig. 1.1 shows a diagram of LHC and its preaccelerators chain, together with the location of the four aforementioned experiments. The LHC is only the final stage in a series of machines used to accelerate the protons to increasingly higher energies. Protons obtained from hydrogen atoms are successively accelerated by four accelerators before being injected inside the LHC: the *Linac2*, a linear accelerator which raises the protons energy to 50 MeV, the *PS Booster* (PSB), the *Proton Synchroton* (PS) and the *Super Proton Synchrotron* (SPS) where they are accelerated to 450 GeV. Inside the LHC, beams of protons travel in opposite directions in separate beam pipes. They are guided around the accelerator ring by a strong magnetic field (8.3 T),

achieved with 1624 super-conducting magnets.
As a consequence of the acceleration scheme, the proton beams are not continuous but circulate the ring in bunches. Under nominal conditions each beam has at maximum 2808 filled bunches over 3564 bunch slots with a minimum spacing of 25 ns, each bunch containing about $1.1 \cdot 10^{11}$ protons.
The LHC was designed to produce collisions with a center of mass energy of $\sqrt{s} = 14$ TeV but, due to an unexpected quench of the super-conducting magnets occurred in 2008, it was decided to run the LHC at reduced energy. In 2010 and 2011, the LHC was operated at 3.5 Tev per beam, and in 2012 the energy was increased to 4 TeV per beam, producing $\sqrt{s} = 8$ TeV collisions. After a shutdown for upgrades, in May 2015 LHC restarted to provide proton collisions and is currently running at $\sqrt{s} = 13$ TeV.
Luminosity is one of the most important operational parameters of an accelerator, being related to the rate of produced interactions: the higher the luminosity, the better. In 2010 the Tevatron proton-antiproton collider at Fermilab reached a peak luminosity at $4 \cdot 10^{32}$ cm^{-2}s^{-1}. The LHC was designed to reach a luminosity two orders of magnitude higher: $1.3 \cdot 10^{34}$ cm^{-2}s^{-1}. The maximum luminosity reached during phase I was: $7 \cdot 10^{33} cm^{-2} s^{-1}$.
Figures 1.2 and 1.3 show the integrated luminosity only provided so far as well as the peak L reached in 2015. Both have been measured using the LUCID detector.

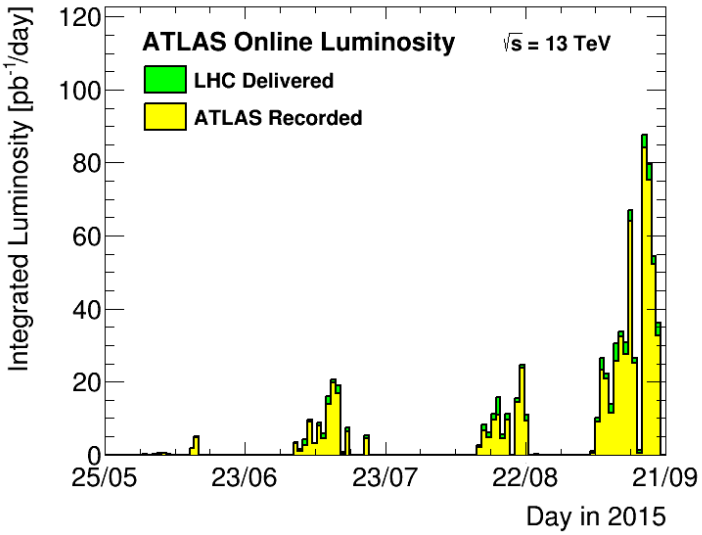

Figure 1.2: Integrated luminosity per day time delivered to (green) and recorded by ATLAS (yellow) during stable beams for pp collisions at $\sqrt{s} = 13$ TeV in 2015.

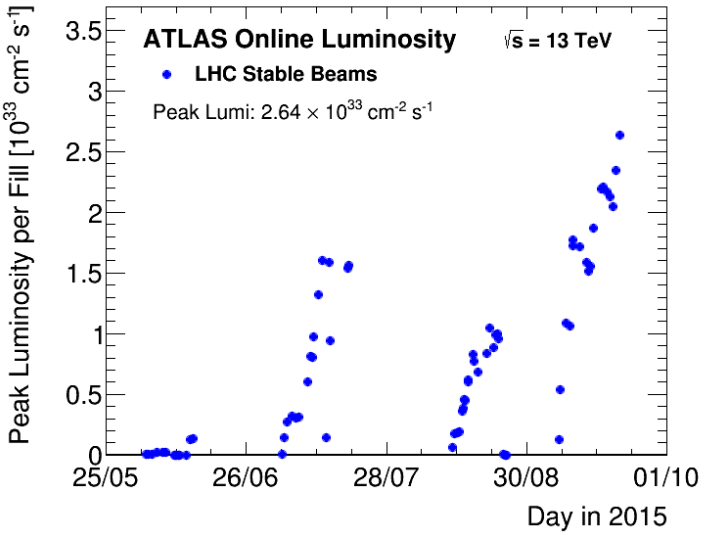

Figure 1.3: The peak instantaneous luminosity delivered to ATLAS during stable beams for pp collisions at $\sqrt{s} = 13$ TeV is shown for each LHC fill as a function of time in 2015.

1.2 The ATLAS Experiment

ATLAS is one of the two general-purpose detectors at LHC [2]. It investigates a wide range of physics, from precision measurements of known phenomena and the search and discovery of the Higgs Boson in 2012, to the search for supersimmetry, extra dimensions and particles that could make up dark matter. The ATLAS detector is centered on one of the LHC collision points. Shown in Fig. 1.4, ATLAS is 46 metres long, 25 metres in diameter, and weighs about 7000 tons. It is split into a barrel part, where detector layers are positioned on cylindrical surfaces around the beam axis, and two end-cap parts, where detectors are positioned in planes perpendicular to the beam pipe.

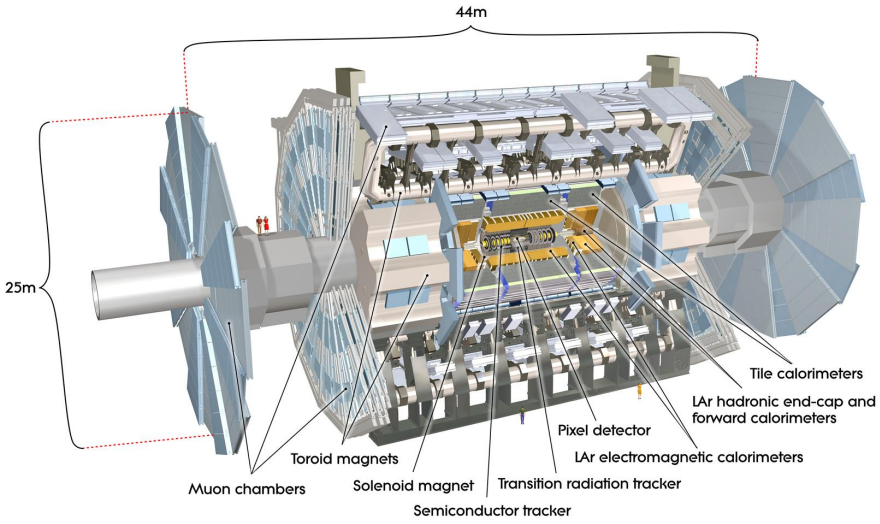

Figure 1.4: Cut-away view of the ATLAS detector showing its various components.

ATLAS is composed of a series of sub-systems, each sensitive to different types of particles produced in the collisions.
The Inner Detector (ID) is the closest to the interaction point and measures the trajectories of charged particles. Surrounding the ID is the calorimeter

system, which is designed to measure the energy of electrons, photons, and hadrons. The Muon Spectrometer (MS) surrounds the calorimeters and is designed to measure the trajectories of high momentum muons escaping the calorimeters.
ATLAS features a hybrid system of three different magnetic fields, each generated by superconductive magnets kept at at temperature of 4.8 K.
The system consists in a central solenoid (CS), which is aligned on the beam axis and provides a 2 T axial magnetic field for the Inner Detector (ID), a barrel toroid (BT) and two end-cap toroids (ECT), which produce toroidal magnetic fields of approximately 0.5 T and 1 T for the muon detectors in the central and end-cap regions, respectively.

1.2.1 Inner detector

The Inner Detector begins a few centimetres from the proton beam axis, extends to a radius of 1.2 metres, and is 6.2 metres in length along the beam pipe. The ID measures the position of charged particles as they traverse the detector. In order to cope with the high particle densities produced by the LHC, the ID has been designed to make high-precision measurements with fine detector granularity. The ID operates in the 2 Tesla magnetic field provided by the solenoid magnet, allowing it to serve as a spectrometer where the particle momentum is measured from the reconstructed curved trajectories. The ID consists of three sub-detectors built using two technologies: silicon sensors and straw drift tubes, as illustrated below:

- **Pixel detector**: it is the innermost part of the detector and originally contained three concentric layers and three disks on each end-cap. During LS1 an additional layer, called Insertable B Layer (IBL), was inserted between the existing detector and a new smaller beam pipe, in order to provide a fourth point for tracing particles, and guarantee the pixel detector not to loose efficiency during the second phase of

operations, in the event a significant radiation damage to the existing layers occurs. The detecting material is 250 μm thick silicon. When charged particles cross the silicon sensors, they generate electron-hole pairs that can be collected with an applied electric field. This charge is recorded locally in the sensor, identifying the position of the particle. The smallest unit that can be read out is a pixel (50 by 400 μm in the older layers and 50 by 250 μm in the IBL); there are roughly 47000 (original layers) or 27000 (IBL) pixels per module, on a total of 2192 modules. The minute pixel size is designed for extremely precise tracking very close to the interaction point, where the particle density is the largest.

- **Strip detector**: it is the middle component of the inner detector. It is similar in concept and function to the Pixel Detector but with long, narrow strips rather than small pixels, thus covering a larger area.

- **Transition-radiation tracker**: the Transition Radiation Tracker (TRT), the outermost component of the inner detector, is a combination of a straw tracker and a transition radiation detector, which also provides electron identification.

1.2.2 Calorimeters

The calorimeters are situated outside the solenoidal magnet that surrounds the Inner Detector. Their purpose is to measure the energy of almost all particles by absorbing them. The calorimeter system provides containment for both electromagnetic and hadronic showers, stopping particles before they reach the muon system.
The *Electromagnetic Calorimeter* (EM) measures the position and energy of electrons and photons. It is a sampling calorimeter with liquid argon as the active medium, which requires a cryostat to keep it at the operating temperature of 87 K, and lead plates as absorber. The lead plates are accordion-shaped to provide full coverage and symmetry without azimuthal

cracks.
The *Hadron Calorimeter* has the task to identify the energy and the direction of particle jets, the result of quarks and gluons hadronization, and hadronically decaying τ leptons. As hadronic showers are longer, wider and have more variance in their development compared to electromagnetic showers, the hadronic calorimeter is much thicker, with an average thickness of ten interaction lengths. For uniformity of the calorimeter and to reduce the radiation background level in the muon spectrometer, a *Forward Calorimeter* (FCal) is integrated into the endcap cryostat. The FCal is split longitudinally in three parts. The absorber material for the first part is made of copper for electromagnetic measurements and the other two parts are made of tungsten for hadronic measurements.

1.2.3 Muon spectrometer

The Muon Spectrometer is an extremely large tracking system, extending from a radius of 4.25 m to the full radius of the detector (11 m), consisting of two parts:

1. A precision system composed of Monitored Drift Tube (MDT) chambers and Cathode Strip Chambers (CSC) measuring the momentum of 100 GeV muons with 3% accuracy, and of 1 TeV muons with 10% accuracy. The MDT chambers are proportional chambers made of aluminum tubes of 30 mm diameter and lengths varying from 70 cm to 630 cm. In the forward region CSCs are used, which are multiwire proportional chambers with a much finer granularity than MTD chambers, making it possible to find tracks in the forward region where the track density is higher compared to the barrel region.

2. Two sets of fast chambers especially developed for trigger purposes: Resistive Plate Chambers (RPCs) in the barrel region and Thin Gap Chambers (TGCs) in the end-caps. An RPC has a gas gap between two resistive bakelite plates with metal strips. A uniform electric field

between the plates creates avalanches when a particle crosses the gas gap, and the induction from the avalanche is measured by the closest metal strips. The 2 mm thick gas-gap gives a fast detector with a 1 ns time resolution allowing individual bunch crossings to be identified. TGCs are multiwire proportional chambers, but with small wire-to-wire and cathode-to-anode distance, giving a time resolution similar to RPCs.

1.2.4 Forward detectors

The ATLAS detector is complemented by a set of detectors in the forward region:

ALFA

The ALFA *(Absolute Luminosity For ATLAS)* detector is located in Roman Pots [3] at 240 m from the interaction point. Its purpose is the measurement of elastic pp-scattering at small angles, down to the Coulomb-Nuclear Interference (CNI) region to measure both the pp cross-section and the absolute luminosity at the ATLAS interaction point. This is done in special LHC calibration runs with large $\beta*$ (amplitude function at the interaction point), special focusing and low instantaneous luminosity. The setup consists of four Roman Pot stations, two on both sides of the interaction point, each housing two vertically movable detectors. In order to measure the impact point of elastically scattered protons each detector is equipped with 1500 scintillating fibres arranged in 20 detection planes, providing a spatial resolution of 30 μm.

BCM

The *Beam Conditions Monitor* (BCM) consists of four small diamond sensors, arranged around the beam pipe in a cross pattern on each side of the interaction point, at a distance of 184 cm. The BCM is a device primarily

designed to monitor background levels and issue beam-abort requests when beam losses start to risk damaging the Inner Detector. The sensors are made of 500 mm thick radiation-hard polycrystalline chemical vapor deposition (pCVD) diamonds. Thanks to its fast readout ($\simeq$ 2 ns shaping time), the BCM also provides bunch-by-bunch luminosity.

LUCID

The LUCID detector *(LUminosity measurement using Cherenkov Integrating Detector)* is the only detector of ATLAS that is completely dedicated to luminosity monitoring. It was built to achieve an uncertainty on $\mathcal{L}$ of better than 5%.

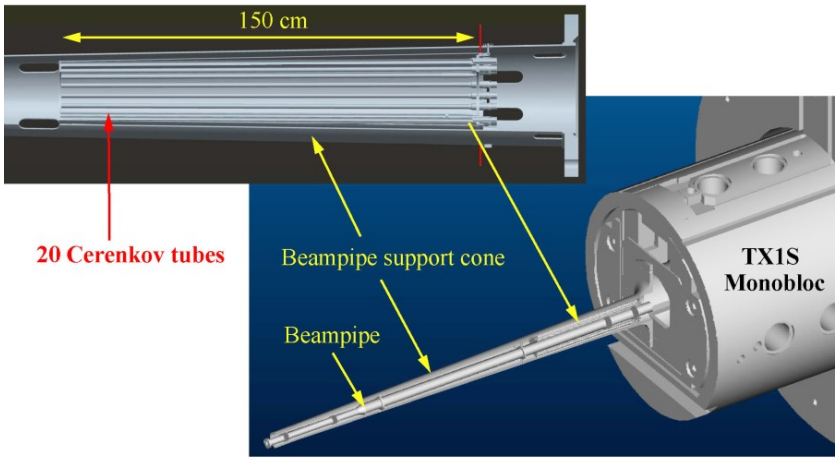

Figure 1.5: Details of the LUCID detector before LS1. In the upper picture the disposition of the 20 Cherenkov tubes is shown.

Before LS1, LUCID consisted of two detector modules that were positioned symmetrically around the beam pipe at about 17 m from the ATLAS interaction point. Proposed when the rest of ATLAS was already designed, it was located in a high radiation area (7 Mrad per year at design luminosity) and was composed of light material, which is intrinsically radiation hard. Each module consisted of 20 aluminium tubes that were arranged along the

beam line, pointing at the IP. The tubes (figure 1.5), 1.5 m long and with a diameter of 15 mm, were filled with a Cherenkov gas radiator (C_4F_{10}) at 1.1 atm, chosen for its high refractive index and transparency to UV photons. Charged particles entering a tube with a momentum larger than the Cherenkov threshold in the gas emit light at an angle of about 3^o with respect to their flight direction. The produced photons undergo reflections on the inner tube walls until they reach the end of the vessel, where they are read out by a photomultiplier (PMT). These PMTs are radiation-hard type, with a quartz window which also produces Cherenkov light. The signals of all PMTs are discriminated and sent to the LUCID readout system where a dedicated card (LUMAT: *LUMinosity And Trigger*) is able to apply fast online luminosity algorithms at the per-bunch level.
In 2015, in order to lower the detector efficiency and migration effects, which will be discussed in section 2.3.4, the Cherenkov gas have been removed, so that Cherenkov light is be produced in the PMT quartz window only. Four different types of sensors are present: four Hamamatsu R760 PMT tubes, four Hamamatsu R760 PMT tubes fit with a Bi207 source for precise calibration, four modified (reduced window size) R760 PMT and four quartz fibre bundles. Fig.1.6 shows the layout of the PMT tubes around the beampipe.
New electronics close to the detectors performs fast signal digitalization guaranteeing a more robust extraction of signal parameters. In addition to the luminosity algorithm described in chapter 2, the new electronics is also able to integrate the charge produced by the PMTs at each bunch-crossing.

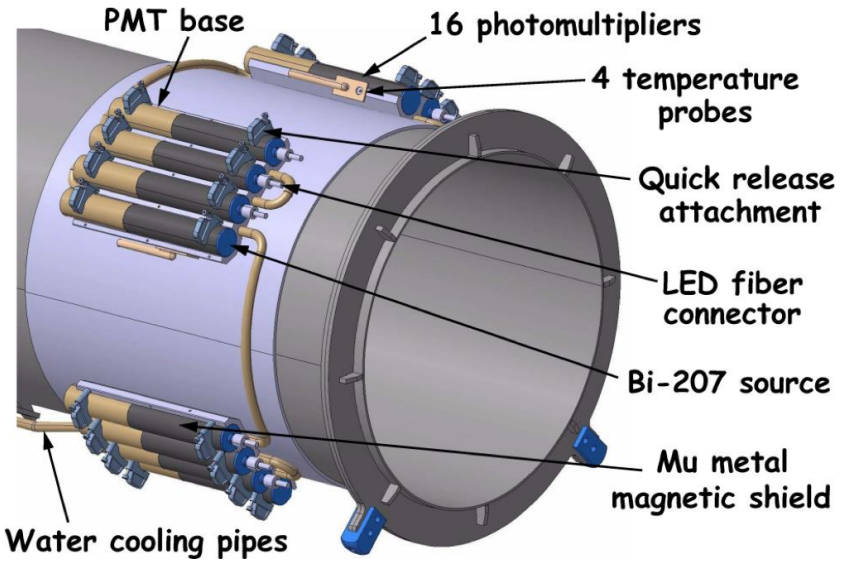

Figure 1.6: The LUCID detector after LS1.

ZDC

The primary purpose of the Zero Degree Calorimeter (ZDC) is to determine the centrality of heavy-ion collisions. It is located 140 m from the interaction point on each side where the two beam pipes merge, exactly on the proton interaction axis. ZDC is composed of two quartz-tungsten sampling calorimeters, each one longitudinally segmented in four modules. Each module (one electromagnetic e three hadronic) contains quartz rods which transport the Cherenkov light produced by incoming neutrons and π^0/γ secondaries to PMTs located on the top of the module for the measurement of the total energy. Some modules have also pixel segmentation for the determination of the position of the electromagnetic and hadronic showers.

Chapter 2

Luminosity determination using ATLAS detector

2.1 Luminosity

The instantaneous luminosity $\mathcal{L}$ of any accelerator is defined as the ratio between the interaction rate R of any process it produces and its cross section σ. It is expressed in units of $\mathrm{cm}^{-2}\mathrm{s}^{-1}$ and it does not depend on the process itself.

$$\mathcal{L} = \frac{R}{\sigma} \tag{2.1}$$

Its precise knowledge is important at LHC since for many cross-sections measurements the uncertainty on the luminosity is the dominant one.
For a circular accelerator, assuming all bunches have the same luminosity (which is usually untrue), instantaneous luminosity can be defined as:

$$\mathcal{L} = \frac{f_r \cdot \mu \cdot n_b}{\sigma} \tag{2.2}$$

where f_r is the beam revolution frequency, n_b the number of bunches, μ the mean number of interactions per bunch crossing and σ is the total cross section.

The instantaneous luminosity can also be inferred from the collider pa-

rameters, as shown in equation 2.3:

$$\mathcal{L} = f_r n_b I_1 I_2 \int \rho_1(x,y)\rho_2(x,y)dxdy \tag{2.3}$$

where f_r is the beam revolution frequency, n_b the number of bunches, I_1 and I_2 the beam intensity, $\rho(x,y)$ is the normalized particle density in the transverse (x-y) plane of beams, and dx and dy the infinitesimal area elements. If the two beams are made of identical bunches, Gaussian in shape and perfectly overlapping without crossing angle, equation 2.3 can be rewritten as:

$$\mathcal{L} = f_r n_b \frac{N_1 N_2}{4\pi\sigma_x\sigma_y} \tag{2.4}$$

where N_1 and N_2 the number of protons in the beam bunches and $\sigma_{x,y}$ are the gaussian transverse profiles of the beams.

The integrated luminosity L is obtained by integrating the instantaneous luminosity over a time interval t and is expressed in units of barns. A barn is defined as 10^{-24} cm^2.

$$L = \int_0^t \mathcal{L}(t')dt' \tag{2.5}$$

At LHC measurements of the integrated luminosity are made over small time intervals, called Luminosity Blocks (LB). The LB is defined as a time interval in which the luminosity can be considered constant. At LHC this corresponds to about 1-2 minute long intervals.

2.2 Luminosity determination

As shown in equation (2.1), the luminosity is the proportionality factor between the rate and cross-section of an observed process. As L is process-independent it is possible to measure the luminosity with any process whose cross-section is known. For a precise luminosity determination, however, it is essential that the process has precise theoretical predictions and at the same time that its rate can be accurately measured.

In contrast to e^+e^- colliders, where the e^+e^- elastic scattering (Bhabha process) used for luminosity measurements is well understood, the main challenge at hadron colliders is to find a theoretically precise and background

free reference process. There are essentially two reasons: the first one is that in strong processes the perturbative corrections are high and difficult to calculate; secondly, that instead of having point like interactions, protons are made of quarks and gluons and the theory describes the interactions between them, so that a precise knowledge of their densities inside the proton is needed.

At LHC, absolute luminosity is not evaluated with equation 2.4, although the beam currents are precisely known, because the gaussian transverse profile of the beams, $\sigma_{x,y}$, cannot be measured with enough precision during physics runs. Therefore, so-called *relative luminosity measurements* are performed by measuring quantities proportional to the inelastic pp rate R_{inel}, as in equation 2.6:

$$\mathcal{L} = \frac{f_r}{\sigma_{vis}} \sum_{i=1}^{n_b} \mu_{vis}^i \tag{2.6}$$

where f_r is the beam revolution frequency, n_b the number of bunches, μ_{vis}^i the mean number of interactions detected per bunch crossing in bunch i and σ_{vis} is the total cross section for inelastic scattering multiplied by the detector efficiency ϵ. μ_{vis}^i are the measured quantities and σ_{vis} is an overall normalization that needs to be determined to obtain absolute measurements. Up to now, dedicated runs with low luminosity called *Van Der Meers Scans* (or *beam separation scans*) have been used to calibrate luminosity monitors with an absolute luminosity determination. This method consists in moving the beams transversely with respect to each other while recording the counting rate of luminosity monitors. Separation scans are performed in both the vertical and horizontal directions. The beam densities contained in equation 2.3 are thus measured and absolute luminosity can be inferred. Since VDM scans are carried out relatively infrequently (in 2011 there was only one set of VDM scans for the entire year), this calibration is applied over long periods and under different machine conditions, requiring the stability of luminosity monitors to be carefully checked.

2.3 Luminosity monitoring in ATLAS

This section provides a description of various quantities used for luminosity monitoring. In order to check the stability and evaluate the systematic uncertainties affecting the main luminosity monitors, the results of several independent detectors are compared [4].

2.3.1 Inner Detector: vertex counting

It is possible to give a luminosity estimate by counting the number of primary vertices produced in inelastic pp collisions. However, vertex counting suffers from nonlinear behaviour with increasing number of interactions per bunch-crossing, which makes it unfit for online monitoring. Moreover, the Inner Detector data must be corrected for deadtime imposed by the CTP (Central Trigger Processor), and bandwidth limitations do not allow to measure the luminosity separately for each bunch pair during normal physics operations.

2.3.2 Calorimeters: total charge

The PMT current drawn in TileCal modules and the charge drawn across the liquid argon gaps in the FCAL modules can also be used for luminosity determination. These charges are proportional to the average particle rate but are only available over rather long time scales, and are thus not on a per-bunch level. Another problem is that an absolute calibration in a VDM scan of these sub-detectors has not been possible up to now, since the luminosity in the scans is below their sensitivity. However, they are cross-calibrated by comparing their currents to an absolutely calibrated measurement of another sub-detector in a high luminosity run taken as reference.

2.3.3 LUCID and BCM: event and hit counting

Signals coming from LUCID and BCM are discriminated providing hits at each bunch crossing. Starting from these hits, various hit and event counting algorithms are implemented, each providing a different μ_{vis}. Events are defined as particular hit patterns. In the following, some of the used algorithms are described in more detail:

- **Event OR algorithm**: an event is counted if there is at least one hit on either of the two detector modules. Assuming that the number of interactions per bunch crossing can be described by a Poisson distribution, the probability of observing an OR event is:

$$P_{OR} = \frac{N_{OR}}{N_{BC}} = 1 - e^{-\mu_{vis}^{OR}} \tag{2.7}$$

  where N_{OR} is the number of events counted over N_{BC} bunch crossing and $e^{-\mu_{vis}^{OR}}$ the probability of observing zero OR events. Solving (2.7) for μ_{vis}^{OR} yields:

$$\mu_{vis}^{OR} = -ln(1 - \frac{N_{OR}}{N_{BC}}) \tag{2.8}$$

- **Event AND algorithm**: a bunch crossing is counted if there is at least one hit on both sides of the detector. Since the formula for the Poisson probability of observing a coincidence can not be inverted analytically, a numerical inversion is performed instead.

At very large L, event counting algorithms lose sensitivity as fewer and fewer events in a given time interval have bunch crossings with zero observed interactions. In the limit where the probability of observing one event per bunch crossing approaches one, these algorithms have no sensitivity at all (algorithm saturation), and different techniques must be used. One example is the **hit counting algorithm**, where the number of hits in a given detector is counted rather than the total of events. Under the assumption that the efficiency of each channel follows a Binomial distribution, and that the number of interactions per bunch crossing follows a Poisson distribution,

one can calculate the average probability to have a hit in one of the detector sensors per bunch crossing as:

$$P_{HIT} = \frac{N_{HIT}}{N_{BC} N_{CH}} = 1 - e^{-\mu_{vis}^{HIT}} \tag{2.9}$$

where N_{HIT} and N_{BC} are the total numbers of hits and bunch crossings during the considered time interval, N_{CH} the number of the detector channels and and $e^{-\mu_{vis}^{HIT}}$ is the probability of observing zero HIT events.

Hit counting was used to analyse the LUCID response only in the high-luminosity data taken in 2011. A study of the LUCID hit distributions shows that the behaviour assumed to derive eq. 2.9 is not correct, as the probability to observe a hit in a single channel is not completely independent of the number of hits observed in the other channels. However, it provides a good description of how μ_{vis}^{HIT} depends on the average number of hits. The efficiency per channel in BCM is lower than in LUCID and event counting algorithm in BCM did not approach their saturation limit yet.
As obvious in equation (2.8), event and hit frequencies are not directly proportional to luminosity. BCID-blind luminosity monitoring, where equal μ_{vis} is assumed in all bunches and the logarithm of averaged rates is evaluated, provides wrong results that must be corrected for. The new LUCID electronics has been designed so as to be able to also measure the charge produced by each PMT at each bunch crossing. New luminosity algorithms based on total charge measurement are currently under study (calibration, stability, etc.).

2.3.4 LUCID performance of RUN I (2010-2012)

In this section LUCID performance during the three years of LHC operation is analysed. From 2010 to 2012 the LHC peak luminosity continuously increased, as can be seen in Fig. 2.1, which depicts the peak instantaneous luminosity delivered to ATLAS over time. In 2010 LUCID provided the best ATLAS luminosity measurement, as it was more sensitive than BCM. The peak instantaneous luminosity was "only" $2.1 \cdot 10^{32}$ cm^{-2}s^{-1}.

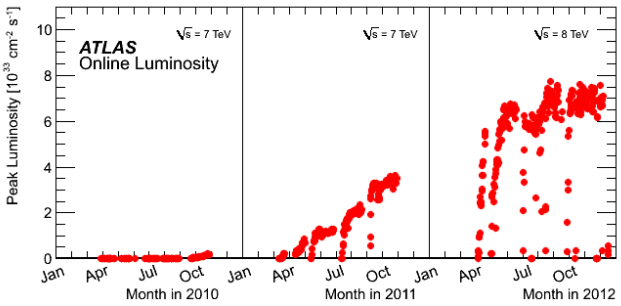

Figure 2.1: The peak instantaneous luminosity delivered to ATLAS per day versus time during the p-p runs of 2010, 2011 and 2012.

From 2011 LHC luminosity increased conspicuously and systematic effects started to appear and had to be corrected for. Still, the final agreement between luminosity measurements of the various monitors was better than 1%: Fig. 2.2 shows a comparison of the LUCID integrated luminosity to the BCM monitor in 2012 runs. The sources of instabilities and systematics were:

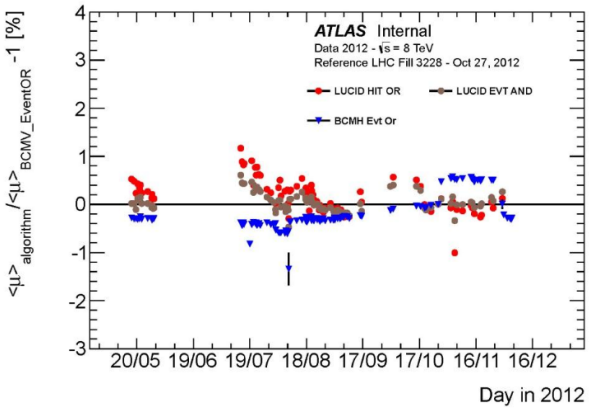

Figure 2.2: Comparison between the LUCID and BCM integrated luminosities in 2012 runs. The agreement is better than 1%.

- *PMTs loss of gain linearity*: high anodic current may cause charge accumulation on the last dynode of the PMT, shielding it, so that the dynodic chain looses linearity. To prevent the loss of linearity, boosters were inserted during the 2011 shutdown to set the potential difference between each pair of dynodes.

- *Migration effect*: when the number of interactions per crossing increases (pile-up), signals, that are individually below threshold, may combine and overtake the threshold, producing a hit. This systematics affects both LUCID and BCM, but it was less relevant for the latter, thanks to its lower acceptance.

- *Saturation*: as mentioned in previous sections, at a certain value of μ, the probability $P_{algorithm}$ that the event condition is fulfilled approaches one. Thus every bunch crossing is counted as an event, which leads to a saturation of the algorithm. Fig. 2.3 shows the saturation of some LUCID algorithms as μ increases. Again, BCM was less affected by saturation because of its lower acceptance.

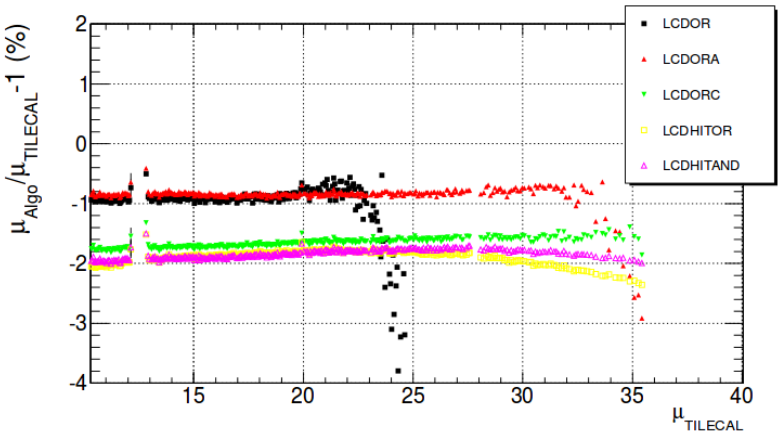

Figure 2.3: Ratio between luminosities measured by LUCID with different algorithms and TileCal, which is not affected by saturation, versus the mean number of interactions per bunch crossing. The Event OR algorithm becomes ineffective for $\mu > 22$, while similar algorithms defined for one LUCID module only (Event ORA and ORC) reach saturation at $\mu > 33$ and 35 respectively. The hit counting algorithms have not saturated at $\mu = 35$ yet. The Event AND algorithm is not depicted in this graphic as there is not enough statistics for high μ, but it is estimated to reach saturation at $\mu \approx 40$.

2.3.5 Upgrade to Phase II

The Long Shutdown 1, dedicated to upgrades and consolidations the super-conducting magnet connections is now over.
Collisions restarted in 2015, and the beam energy is currently 6.5 TeV per beam. Instantaneous luminosity is also expected to be doubled soon. To achieve an increase in luminosity, the number of filled bunches will be doubled and the proton density increased with a greater focusing at the IP. The latter, together with doubled beam energy, leads to an increase of the mean number of interactions per bunch crossing. Table 2.1 show the overall expected effects of the upgrade, with a comparison between some LHC

parameters in Phase I and II.

Parameter	Phase I (peak)	Phase II (expected)
Center of mass energy	8 TeV	13 TeV
Instantaneous luminosity	$7 \cdot 10^{33}$ cm^{-2}s^{-1}	$1.3 \cdot 10^{34}$ cm^{-2}s^{-1}
Number of filled bunches	1380	2808
Bunch time spacing	50 ns	25 ns
Mean number of interactions per b.c.	35	50

Table 2.1: LHC working parameters in Phase I and II

During the shutdown several detectors underwent hardware and electronics upgrades. As far as LUCID is concerned, the main upgrades and changes will be now listed.

1. LUCID has been moved nearer to the interaction point, as the Cherenkov tubes are no longer necessary. This area is less radioactive because farther from the TAN absorber, which produced most of the secondary emissions that affected LUCID.

2. A new electronic card equipped with FADCs for charge integration over 25 ns intervals has been designed and installed. Its purpose is to complement the Event Counting algorithms with measurement of the total charge, to solve the problems caused by the migration effect, as this method does not involve any thresholds, and to provide a robust BCID-blind and fast luminosity monitoring.

3. PMTs have been replaced because of their ageing during Phase I.
   The PMTs lifetime strongly depends on the total integrated charge they accumulate during their functioning. In particular, the last dynode near the anode deteriorates because of the continuous electron collisions. The maximum current supported by a PMT during its lifetime is not specified in its construction parameters, but it is estimated to be about 500 C. During the three years of operation of Phase I, the total

charge sustained by the PMTs was about 750 C. During Phase II an integrated luminosity of 50 fb^{-1} per year is anticipated, and the PMT would produce about 2500 C if operated for three years at the same gain as in Phase I, far more than they can bear.

Another possible cause of PMT degradation is the absorbed radiation, but the installed PMTs were still functioning at the end of Phase I, and showed no deterioration effects. Indeed, prior to installation, the PMTs had been tested for gamma ray and neutron hardness, with a procedure similar to the one illustrated in Chapter 4. The PMTs passed the testing with an irradiated dose 30 times larger than the absorbed one during Phase I, without any noticeable effect except for a Dark Current increase.

As a PMT replacement was nevertheless necessary in view of the total charge to be produced, it was decided to change the PMT model as well, opting for a smaller one to reduce the PMT acceptance and efficiency. This, together with a different working point (lower gain), was predicted to mitigate the problems that affected LUCID during operation at high luminosity in 2011-2012. The two possible models considered to replace the previously employed Hamamatsu R762 are the models R2496 and R760 by the same producer, illustrated in more detail in section 3.3.

The final choice was for model R760.

2.3.6 LUCID performance in 2015 with first beams

Lucid is currently the preferred luminosity monitor in ATLAS, both for online instantaneous luminosity monitoring and offline analysis.
Since August, LHC is operating at 25 ns bunch spacing. The BCM electronics is apparently unable to cope with such a rate, loosing up to 15% in contiguous BCID within bunch trains. LUCID and BCM counts are still in agreement on isolated bunches. In addition, the luminosity measured by LUCID after integration over all bunches is in agreement with the luminosity measured by te calorimeters, that are not affected by the reduced bunch spacing, as their measurements are BCID blind.
The preferred algorithm for online luminosity is event AND, based on the sensors equipped with a Bi207 source for precise calibration, while the preferred algorithm offline is event OR A. Charge algorithms are still in a commissioning phase.

Chapter 3

Photomultipliers

3.1 Principles of operation

Photomultipliers are electron tube devices which convert light within and near the visible range into a measurable electric current [5].
They consist of a cathode made of photosensitive material followed by an electron collection system, an electron multiplier section (usually called dynode string) and finally an anode from which the final signal can be taken. All parts are usually housed in an evacuated glass tube. Fig.3.1 shows a schematic diagram of a typical photomultiplier.

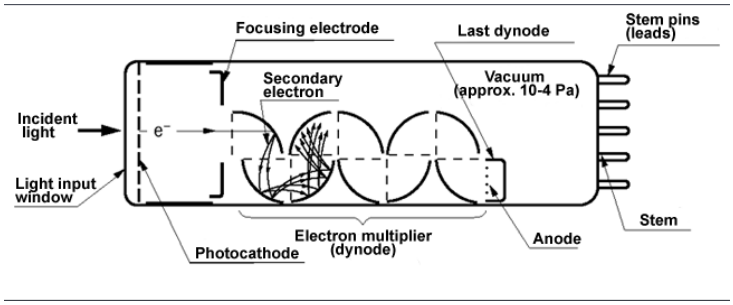

Figure 3.1: schematic diagram of a photomultiplier tube.

When an incident photon collides on the photocathode, an electron can

be emitted via photoelectric effect. Because of the high applied voltage, the electron is then accelerated toward the first dynode, where it transfers some of its energy to the electrons in the dynode. This causes secondary electrons to be emitted, which in turn are accelerated towards the next dynode, thus creating an electron cascade down the dynode string. At the anode the cascade is collected to give a current which can be amplified and analysed. What follows is a brief description of the single parts and their required characteristics [6]:

Input window: it is the first component met by the incident light. The window material limits the spectral sensitivity in the short wavelength region and, when working in a high-radiation environments, needs to be resistant to radiation. The most used materials are: borosilicate glass, the cut-off wavelength of which is 270 nm and it is not radiation resistant; UV-quartz, which transmits light down to 185 nm and it is radiation resistant.

Photocathode: it is the thin layer deposited on the inside of the PM window where the incident light does photoelectric effect. The material of the photocathode sets the upward limit on the wavelength of the detectable incident light as a certain minimum frequency is required for the photoelectric effect to take place. Most of the photocathodes are made of bialkali, which require few eVs for an electron to be extracted and are responsive up to 630 nm, or, equivalently, 1.97 eV.

Dynodes: electrons emitted from the photocathode are multiplied using a series of secondary emission electrodes, called dynodes, to produce a measurable current at the anode. Common photomultipliers contain 8 to 12 dynodes, arranged in a wide range of configurations in order to maximize the photomultiplier efficiency.

3.2 Operating Parameters

3.2.1 Gain

The photomultiplier gain is defined as the ratio of the output signal current to the photoelectric signal current from the photocathode.

$$G = \frac{I_{anode}}{I_{photocathode}} \tag{3.1}$$

Assuming the applied voltage is equally divided among the dynodes, gain can be expressed as δ^n, where n is the number of dynodes and δ is the secondary emission factor. The latter is a function of the energy of the primary electron, which is, in a multiplier chain, a function of the potential difference between the dynodes. Therefore we can write:

$$\delta = A \cdot \Delta V^{\alpha'} \tag{3.2}$$

where A is a constant, ΔV is the potential difference between the dynodes and α' a parameter determined by the dynodes configuration and material. Given the total applied voltage $V = (n \cdot \Delta V$, the overall gain of the PMT becomes:

$$G = \delta^n = (A \cdot \Delta V^{\alpha'})^n = [A(\frac{V}{n})^{\alpha'}]^n \tag{3.3}$$

$$= \frac{A}{n^{\alpha' n}} V^{\alpha' n} = K V^{\alpha' n} = K V^{\alpha} \tag{3.4}$$

where K is a constant and α is the gain parameter.

3.2.2 Dark Current (DC)

Output current from a photomultiplier is obtained even in the absence of incident light. This current is called Dark Current and is a pivotal parameter to determine the minimum energy detectable by a photomultiplier. DC arises from several sources:

- **Thermionic emission**: since the photocathode and dynode surfaces are composed of materials with a very low work function, they emit

thermionic electrons even at room temperature. At a given temperature, the thermionic effect exponentially increases with the supply voltage.

- **Ohmic leakage**: A leakage current may be generated between the anode and the last dynode inside a tube. It may also be caused by imperfect insulation of the glass stem and base, and between the socket anode pin and other pins. It is a major part of dark current when a PMT is operated at low gain ($< 10^4$) or at low temperature.

- **Scintillation from the glass envelope or electrode support materials**: some electrons emitted from the photocathode or dynodes may deviate from their normal trajectory and impinge on the glass envelope, causing scintillation.

- **Field emission**: if a photomultiplier tube is operated at an excessive voltage, electrons may be emitted from the dynodes by the strong electric field. Subsequently the dark current increases abruptly and the life of the photomultiplier tube shortens considerably.

- **Ionization current of residual gases**: The molecules of the residual gases inside a photomultiplier tube may be ionized by collision with electrons. The positive ions that strike the front stage dynodes or the photocathode produce many secondary electrons, resulting in a large noise pulse. This is usually identified as an output pulse appearing slightly after the main photocurrent, therefore called *afterpulse*.

- **Activation of photomultiplier material**: a high-radiation environment may cause the photomultiplier material itself, especially aluminum, to become radioactive and produce noise. This is notably relevant in LUCID working environment.

3.2.3 Spectral response

The photocathode of a photomultiplier converts the energy of incident photons into photoelectrons. The conversion efficiency (photocathode sensitivity) varies with the incident light wavelength. This relationship between the photocathode and the incident light wavelength is referred to as the spectral response characteristics. The spectral response range is determined by the photocathode material on the long wavelength edge, and by the window material on the short wavelength edge.

3.2.4 Time response

During Phase II, LUCID has have to single out signals with a 25 ns spacing, and photomultiplier tubes were chosen because they typically have a fast time response. The response of a photomultiplier to a delta pulse of light is governed by the electron trajectories within the tube. Photoelectrons created by the light pulse follow individual path to the first dynode, depending on their point of origin on the photocathode and on their emission velocities. It follows that they land on the first dynode at different points and different times. Secondary electrons travel individual paths between dynodes, causing further time dispersion. Thus smaller PMTs have a better time response and resolution, as shorter distances between dynodes allow less dispersion. A photomultiplier output pulse is characterised by:

- *rise time*: it is defined as the time for the output pulse to increase from 10 to 90 percent of the peak pulse height, when the photocathode is illuminated with a delta function-like source. Conversely, the *fall time* is defined as the time required to decrease from 90 to 10 percent of the peak pulse height;

- *electron transit time*: it is the time interval between the arrival of a light pulse at the photocathode and the the instant the output pulse of the multiplier reaches its peak amplitude;

- *transit time spread*: it is defined as the full-width-at-half-maximum of the time distribution of a set of pulses each of which corresponds to the photomultiplier transit time for that individual event.

The time response is mainly determined by the dynode type, but also depends on the supply voltage. Increasing the electric field intensity or supply voltage improves the electron transit speed an thus shortens the transit time.

3.2.5 Linearity

The linearity of a multiplier is defined as the degree of proportionality between the number of electrons collected at the anode and the number of incident photons. It is important to know within what extents a photomultiplier can still be considered linear. The linearity depends strongly on the type of dynode configuration and the current in the tube. In general, photomultiplier linearity requires that the current at each stage be entirely collected by the following stage, and current collection depends on the voltage difference applied between stages. If the incident light is too large, the output begins to deviate from the ideal linearity. This is primarily caused by space charge effects due to a large current flowing through the dynodes.

3.2.6 Stability

The output variation of a photomultiplier tube over short time periods are referred to as drift, while variations over spans of time longer than 10^3 to 10^4 hours are referred to as the life characteristics. The drift and life characteristics primarily depend on variations in the secondary emission ratio. In other words, they indicate the extent of gain variation with operating time. One of the main causes of instability of a PMT on a long term is the dynodes degradation: it is estimated that a PMT can sustain up to 500 C integrated charge during its lifetime.

3.3 PMT models for Phase II

Two photomultiplier tube models were initially selected as candidates to replace the Hamamatsu R762 employed in LUCID during Phase I. Both were selected among the PMTs with a quartz window produced by Hamamatsu, as quartz is radiation resistant, and both have a smaller window than R760, thus having a smaller acceptance in order to reduce the systematic effects discussed in section 2.3.4.

- *Hamamatsu R760*: it is the smallest variant of Hamamatsu R762. It has a 10 mm diameter window whereas the R762 is 15 mm wide. Its multiplier chain consists in 10 dynodes, the window shape is planar and 1.2 mm thick. The photocathode is made of bialkali.

- *Hamamatsu R2496*: it is the smallest PMT with a quartz window produced by Hamamatsu. Like R760, this model has a photocathode made of bialkali, but the window shape is planar-concave and smaller (8 mm). Because of its size and multiplier chain, which consists in 8 dynodes instead of 10, it also has a faster time response than R760.

A list of construction parameters of both models follows in table 3.1 [7].
Before choosing the PMT model to install in LUCID, both needed to undergo resistance tests for gamma ray and neutron radiation. Indeed, it was necessary to check their stability when subjected to doses akin to the ones expected during Phase II.
The neutron radiation resistance tests are the subject of this thesis and will be illustrated in the next chapter.

Model	R760	R2496
Tube size (diameter)	13 mm	10 mm
Photocathode area size (diameter)	10 mm	8 mm
Photocathode area shape	planar	plano-concave
Dynode stages	10	8
Wavelength (short)	160 nm	160 nm
Wavelength (long)	650 nm	650 nm
Wavelength (peak)	420 nm	420 nm
Photocathode material	Bialkali	Bialkali
Window material	Quartz	Quartz
Cahtode Luminous sensitivity (typical)	110 μA	100 μA
Max voltage	1250 V	1500 V
Max anodic current	100 μA	30 μA
Gain typ.	10 E6	10 E6
Dark current after 30 min typ.	1 nA	2 nA
Dark current after 30 min max	15 nA	50 nA
Rise time typ.	2.1 ns	0.7 ns

Table 3.1: Technical specifications of PMT R2496 and R760

Chapter 4

Neutron radiation resistance tests on PMTs

This chapter illustrates the measurements conducted at the Physics Department of the University of Bologna to test the resistance to neutron radiation of PMT models Hamamatsu R760 and R2496.
For this purpose, two PMTs were bought per model. The operating parameters that are the most likely to be affected by radiation were measured: the *dark current*, *spectral response*, the gain parameter α defined in 3.2.1 and hereafter referred to as *relative gain*, and the *absolute gain*. Then, a PMT per model was irradiated, while the other was kept as reference to control the stability of the experimental setup. After irradiation, the parameters previously mentioned were measured again and results were compared to establish the PMT resistance.

The PMTs EA3360 and VA1601 (Table 4.1) were irradiated with a fluence of $2.7 \cdot 10^{14}$ neutrons/cm^2, equivalent to the one expected for the LHC running during years 2015-2017, at the ENEA Laboratory in Casaccia, Rome, on the 22^{nd} of November, 2013. Measurements of the PMT parameters had been performed during the first week of November and, after irradiation, they were repeated over the span of two and a half months, from the 17^{th} of December until late February. The candidate participated to the measurements per-

Model	PMT serial number	employment
R760	EA3360	irradiated
R760	EA3359	reference
R2496	VA1601	irradiated
R2496	VA1599	reference

Table 4.1: The four PMTs tested in this thesis. For each model, a PMT was irradiated and the other was used as a reference.

formed after neutron irradiation, analysed the results and compared them to the ones obtained before irradiation.
In September 2013, the same PMTs subjected to neutron irradiation had been tested for gamma ray radiation, without any significant variation in their characteristics but an increase of dark current.

4.1 Experimental setup

Each PMT was placed inside a black box where the photocathode could be illuminated by a light source thanks to an optical fibre, and the PMT was powered by an external power supply. Two different setups were used depending on the measurement to be performed.
A schematic view of the experimental setup used for measurements of DC, spectral response and relative gain is shown in Fig. 4.1. Fig. 4.2 shows the alternative setup used for measurements of absolute gain. In both cases, the apparatus is made of:

- A light source, either a xenon lamp complemented by a monochromator or an LED (green or red). Most measurements were taken using the xenon lamp;

- A multi-mode optical fibre to transmit light from the source to the PMT window;

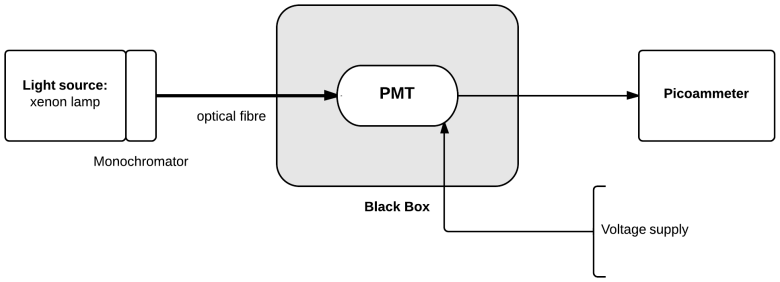

Figure 4.1: Schematic view of the experimental setup for DC, spectral response and relative gain measurements.

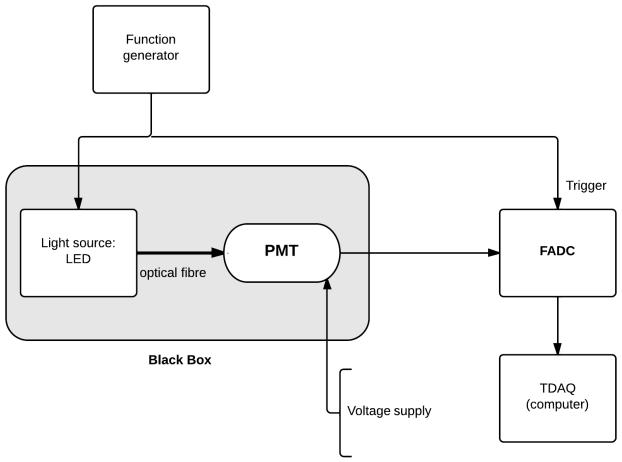

Figure 4.2: Schematic view of the experimental setup for measurements of single photoelectron spectra.

- A black box: a black-painted, wooden box wherein the PMT was placed. During measurements the box was clad in aluminium foil and covered by thick dark fabric to provide electromagnetic and light shielding. Supply voltage and LEMO cables as well as the optical fiber enter the box through small holes, sealed with black tape;
- A High Voltage power supply for the PMT: CAEN N1740;

Measurements of currents were performed with a digital picoammeter (KEITHLEY mod. 6485), with a sensitivity down to 20 fA and resolution of 10 fA at 2 nA scale. For each measurement, the picoammeter registered 100 values of anodic current, returning their mean value and standard deviation. The returned values are used for data analysis in this chapter. During absolute gain measurements using the single photoelectron technique (Sect. 4.5), the picoammeter was replaced by a FADC (Flash Analog to Digital Converter) CAEN v1720, a VME board with the function of a digital oscilloscope that samples the incoming signal every 4 ns. The trigger signal was provided externally by a pulse generator (Textronix AFG3000C), also feeding an LED with a short square pulse. Data sampled by the FADC was then read out by the ATLAS TDAQ (Trigger and Data Acquisition) software, including an online algorithm for charge integration, providing charge distribution histograms for further analysis.

The laboratory temperature was controlled with air conditioning, as the dark current is strongly influenced by temperature.

4.2 Measurements and data analysis

For each measurement session, PMTs were turned on several hours beforehand, as they need time to adjust. When a variation of anodic voltage was made, we always waited several minutes between one measurement and another. Also, we did not vary anodic voltage more than 100 V per time, as wide leaps of supply voltage require more time for adjusting.

4.2.1 Dark Current (DC)

Dark Current measurements were taken with the experimental setup described in Fig. 4.1, but without any light source.
Fig. 4.3 shows the DC as a function of HV for the irradiated PMTs (right column) next to their reference one (left column), before and 25 days after neutron irradiation. It was not possible to make earlier measurements as the PMTs were not released from the irradiation facility before.
Points represent the average of the 100 measurements performed by the picoammeter at each value of the supplied voltage. Error bars represent the statistical error on the average.
Differences between the measurements of the reference PMT provide a taste of the reproducibility of experimental conditions before and after irradiation. Even before neutron irradiation, the DC of the PMT under test was higher than that of their reference, due to previous irradiation with gamma rays. However, a further DC increase by about one order of magnitude for PMT EA3360 (model R760) was observed after neutron irradiation. The DC of PMT VA1601 was overall higher than that of PMT EA3360, although the relative increase due to neutron irradiation is lower.

Nonetheless, at LUCID working voltage, about 800 V, the DC does not exceed 1 nA for both PMTs before and after irradiation. Considering that during LHC operation the PMTs current is about two or three orders of magnitude higher, depending on the number of filled bunches, the measured DC is negligible.

DC measurements have been repeated over two months, observing a decay of DC over time in both irradiated PMTs. In particular, Fig. 4.4 shows several voltage scans for PMT EA3360 and Fig. 4.5 shows the DC trend over time for both PMTs at 800 V.

Estimating a realistic recovery time of the PMTs in LHC working conditions is not possible, as in our test the expected three-year dose was provided in just a few days. However one can observe that after about 65 days EA3360

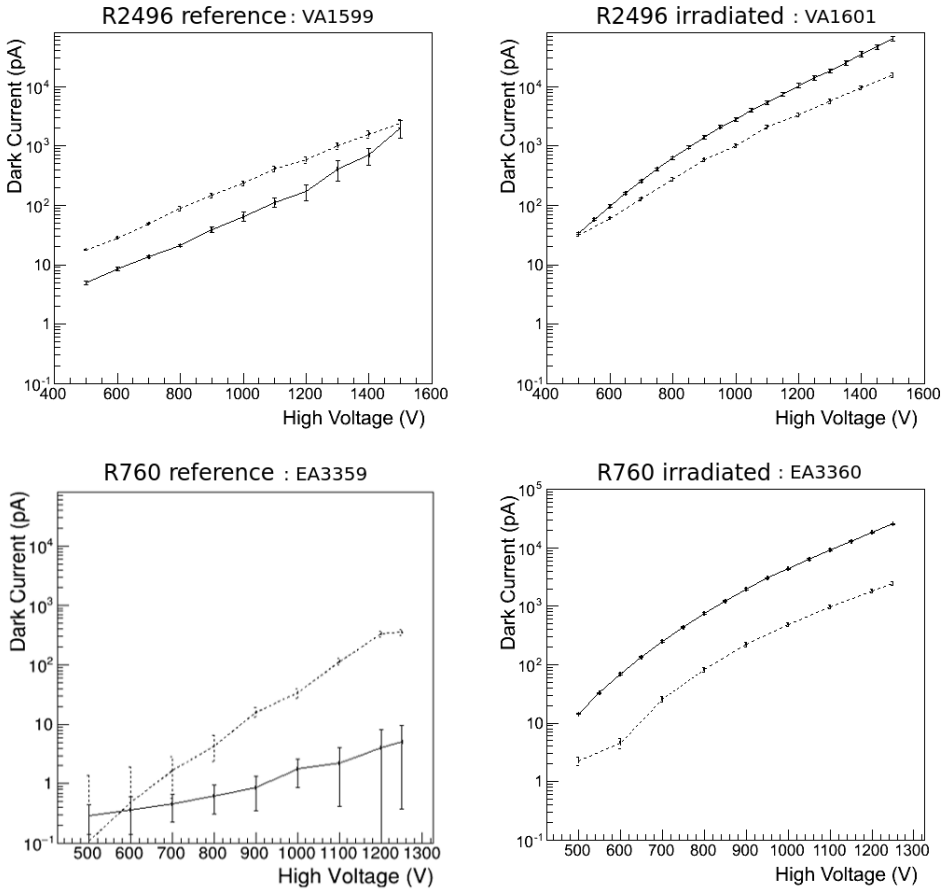

Figure 4.3: Dark Current versus supply voltage for PMT model R2496 (top) and R760 (bottom). Dashed lines refer to measurements before EA3360 and VA1601 irradiation, solid ones to measurements afterwards. The DC of VA1601 and EA3360 is larger than the one of VA1599 and EA3359 even before neutron irradiation due to a previous gamma irradiation.

DC values are similar to the ones before neutron irradiation, while VA1601 appears slower in its recovery, needing about 80 days (Fig. 4.5). Considering that the radiation absorbed in Phase II will be distributed over a much longer time - with pauses during the machine development weeks and Christmas closure - recovery times of about two months are not at all worrisome.

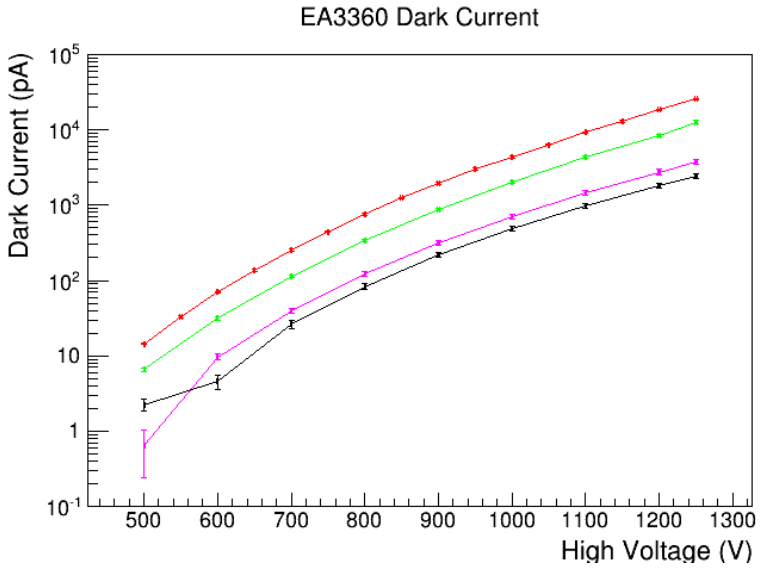

Figure 4.4: DC versus supply voltage for PMT R760 EA3360. Measurements were taken 15 days before irradiation (black line), 25 days after irradiation (red), 46 days (green) and 67 days (purple) after irradiation.

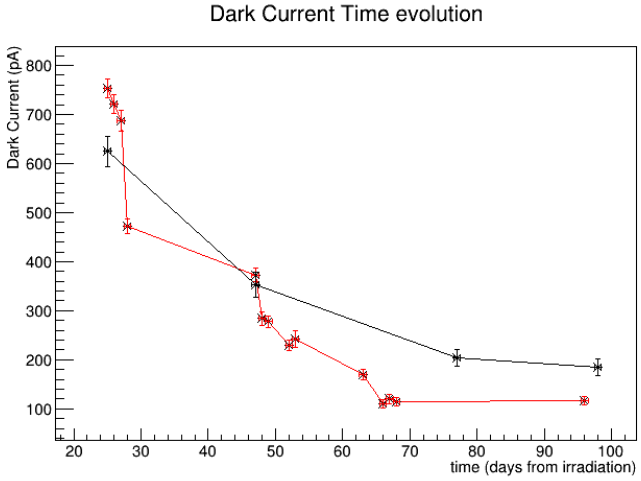

Figure 4.5: Time evolution for DC at 800 V for PMT VA1601 (black line) and EA3360 (red).

4.2.2 Spectral response

The spectral response, that is the relationship between the cathode sensitivity and the incident light wavelength, is another characteristic that may change with irradiation. An absolute evaluation of the PMTs spectral response is not possible - it would require a constant light intensity for the whole wavelength range used, as well as an optical fibre with transmission efficiency independent of the wavelength - and not needed for this thesis purposes, where looking for differences induced by radiation is enough. Indeed, it is sufficient to study the dependence of the current drawn by the PMT as a function of the wavelength selected by the monochromator shown in Fig. 4.1, before and after neutron irradiation, and look for variations. Current measurements were taken with the PMT supply voltage fixed at 800 V.
The anodic current as a function of wavelength, measured before and after neutron irradiation, has been normalized to the value at 475 nm, as shown in Fig. 4.6 and 4.7 for both the irradiated PMT and the reference one. The DC was subtracted from all current measures before normalizing. Only statistical errors are shown.

For the irradiated PMT of model R760, i.e. EA3360, no significant variation of the effective spectral response is observed in the wavelength range of 300-650 nm. At the extremes of the sensitive range, where the DC is of the same order of magnitude of the measured current, data before and after irradiation are not consistent within their errors. The limited control on the temperature of the room when the measurements were taken is most likely responsible for this behaviour. For the other irradiated PMT, of model R2496, agreement between data before and after irradiation is restricted in the range from 400 to 800 nm. Still, it is not possible to assert that this variation in the effective spectral response is caused by the irradiation, as a variation in that wavelength range is also present in the reference PMT VA1599.
Fig. 4.8 shows ratios between normalized currents before and after irradia-

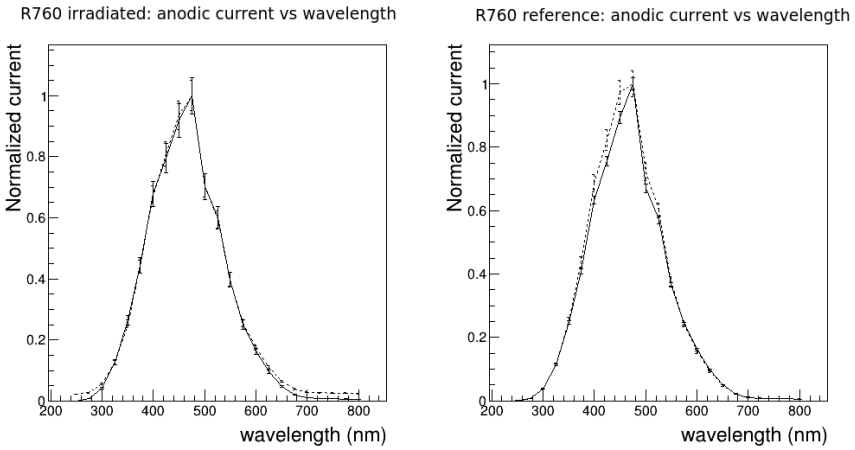

Figure 4.6: Measured anodic current as a function of wavelength, normalized to the one at 475 nm, for the irradiated PMT (EA3360, left) and the reference one (EA3359,right). Dashed lines refer to measurements made in November, prior to the neutron irradiation, and solid ones to measurements in January. Only statistical errors are displayed.

tion for all PMTs, both the irradiated ones (solid line) and their reference (dashed line). These ratios indicate that the experimental conditions were not always stable. However, as both irradiated PMTs behave similarly to their reference ones, we conclude that no real effect is observed within a precision of about 10%.

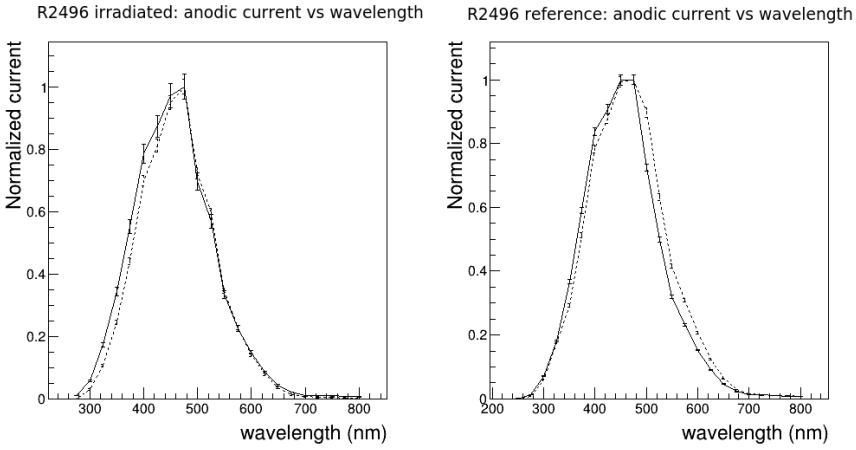

Figure 4.7: Measured anodic current as a function of wavelength, normalized to the one at 475 nm for the irradiated PMT (VA1601, left) and the reference one (VA1599, right). Dashed lines refer to measurements made in November, before irradiation, solid ones to measurements performed in February. Only statistical errors are shown.

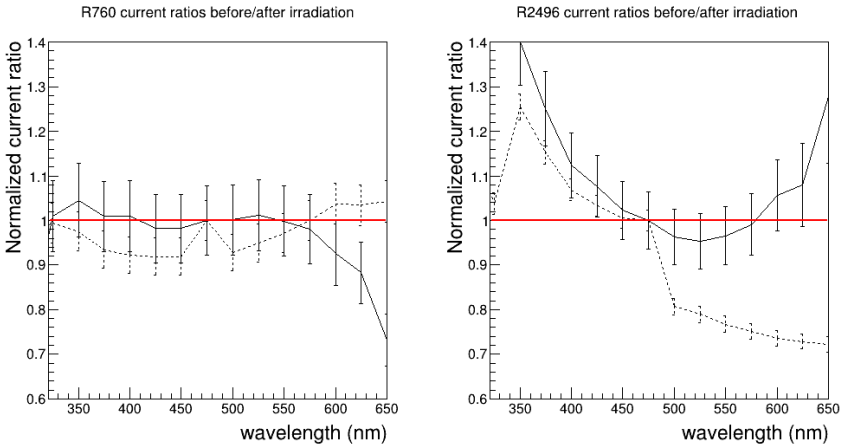

Figure 4.8: Ratios of normalized current after/before irradiation, for PMT models R760 (left) and R2496 (right). Solid lines refer to the irradiated PMTs, dashed lines to the reference ones. The red line indicates the expected ratio in case of no effects. The wavelength range is restricted to $350 < \lambda < 650$ nm, as dark current dominates over anodic current outside this interval.

4.2.3 Relative gain

As mentioned in section 3.2.1, the photomultiplier gain G depends on the applied voltage V according to a power law:

$$G = KV^{\alpha} \tag{4.1}$$

Where K and α are constants. Without knowing the exact amount of cathodic current we cannot measure the absolute gain of a PMT. However, using a constant incident light, we can estimate the α parameter in equation (4.1) by considering ratios between currents measured at different voltages. These ratios are in fact equal to the gain ratios as gain is proportional to the anodic current.
Using the measured current at 1000 V as reference, we can write:

$$\frac{I_V}{I_{1000}} = \frac{G_V}{G_{1000}} = (\frac{V}{1000})^{\alpha} \tag{4.2}$$

Where I_V is the current measured at the HV supply voltage V and G_V is the corresponding gain.
By taking the logarithm of both sides of equation (4.2), a straight line is obtained, whose slope is the α parameter we are to measure.
For α measurements either an LED or the xenon lamp can be used as light source, provided they are stable. The former can be set to emit a pulsed light signal that mimics the PMT behaviour in the LHC, where light is produced by charged particles traversing the PMT window, while the latter has a continuous light output.
Both sources produced consistent results, but the xenon lamp was preferred and used for most of the measurements as the PMTs became saturated at high voltages when the 1 kHz LED signal was set ample enough to obtain measurable currents at the lowest supply. Of course, we might have decreased the amplitude of the LED signal wile increasing its frequency to avoid saturation on single pulses, but such thing was not considered necessary given the consistency of results at low power supplies.
The light emitted by the xenon lamp has a continuous spectrum and was

filtered by the monochromator to select a wavelength of 500 nm, as it is close to the peak of sensitivity of the PMTs.

We performed current measurements while doing two voltage scans: first from the maximum voltage supported by the PMT (1250 V for the R760 model and 1500 V for the R2496) to 500 V, with a step size of 100 V, and then in the opposite direction, from 500 V to the maximum value.

A typical set of current measurements taken after irradiation for EA3360 is shown in table 4.2.

HV (V)	**I (nA)**	σ **(nA)**
1250	614	3
1200	442	2
1100	235.6	1.6
1000	114.7	0.7
900	50.7	0.3
800	29.98	0.12
700	6.47	0.04
600	1.929	0.012
500	0.427	0.003
600	1.901	0.013
700	6.64	0.04
800	19.20	0.10
900	48.16	0.3
1000	107.5	0.7
1100	218.6	1.5
1200	412	2
1250	552	3

Table 4.2: Measured PMT current as a function of voltage supply in presence of a 500 nm light source for PMT EA3360.

To take into account effects due to instabilities in the light source and the time needed to stabilize the PMT after a HV change, two different linear fits were performed: one when lowering the voltage, and one when rising it. Differences between the fitted values of α were taken as systematics. This procedure had not been followed for the measurements performed before neutron irradiation, for which only statistical errors are available. Moreover, fitting was done both on the whole HV range and from 500 to 1000 V, to reduce any possible effect of non-linearity at high voltages.
The fit χ^2 values resulted rather high, probably due to instabilities in the light source. Thus we imposed the validity of (4.2) and increased all relative errors on the currents by the same factor (approximately 50% when fitting on the whole HV range, and 30% on the 500 - 1000 V range) until a χ^2/ndf ratio close to 1 was reached. Fig. 4.9 shows as an example the fits done for PMT EA3360.

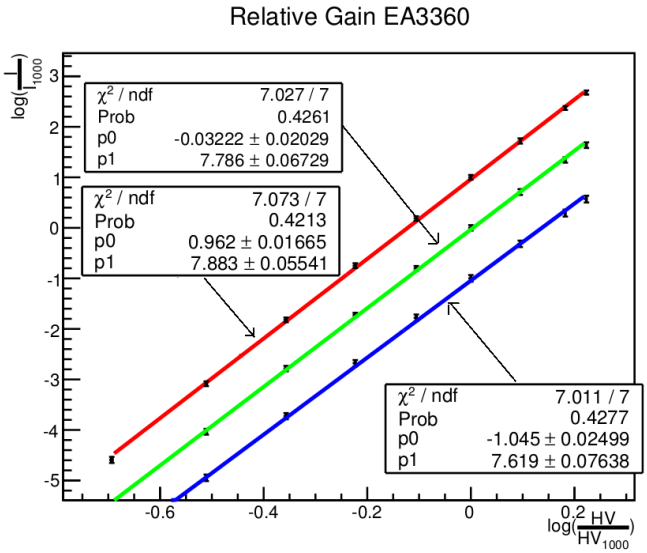

Figure 4.9: R760 EA3360. Blue line: scan before irradiation. Red line: scan after irradiation, lowering voltage. Green line: scan after irradiation, rising voltage. Red and Blue lines are vertically shifted for an easier reading.

Fitted values of α after irradiation are summarized in table 4.3. For the two HV scans, each pair of α values referring to the same voltage range are consistent within 1.5 times the statistic error. The mean of each pair of values is then taken as a central value, to which we assign half their difference as further systematic error, summed in quadrature to the statistical one. In table 4.4 the final results are compared with the relative gain values measured before irradiation.

PMT	**HV range**	$\alpha_1 \pm \sigma_{fit}$ (rising voltage)	$\alpha_2 \pm \sigma_{fit}$ (lowering voltage)
R760 irradiated	500-1250 V	7.78 ± 0.06	7.88 ± 0.06
R760 irradiated	500-1000 V	7.97 ± 0.05	8.06 ± 0.05
R760 reference	500-1250 V	7.73 ± 0.05	7.79 ± 0.06
R760 reference	500-1000 V	7.88 ± 0.05	7.97 ± 0.05
R2496 irradiated	500-1500 V	6.40 ± 0.02	6.49 ± 0.03
R2496 irradiated	500-1000 V	6.47 ± 0.03	6.56 ± 0.05
R2496 reference	500-1500 V	5.65 ± 0.05	5.76 ± 0.03
R2496 reference	500-1000 V	5.81 ± 0.03	5.87 ± 0.02

Table 4.3: Relative gain values as obtained by separated fits for each PMT and voltage range.

A small increase of the α values of the irradiated PMTs is observed in all fitting ranges. The difference between α values (stated as "shift" in table 4.4) of model R760 is slightly bigger than 1σ, while for model R2496 it is about 3σ. However, when fitting from 500 to 1000V, which is the HV range of major interest of LUCID, a difference larger than 2σ is present in the reference PMT for model R2496 as well, pointing to some systematics not completely under control. We therefore conclude that no significant variation of the PMTs gain is observed within the precision of our measurements (better than 5%).

		before irrad.	**after irrad.**	**shift**
PMT	HV range	$\alpha \pm \sigma_{fit}$	$\alpha \pm \sigma_{fit+sys}$	$\Delta\alpha \pm \sigma$
R760 irr.	500-1250 V	7.62 ± 0.08	7.83 ± 0.08	0.21 ± 0.16
R760 irr.	500-1000 V	7.83 ± 0.06	8.01 ± 0.07	0.18 ± 0.13
R760 ref.	500-1250 V	7.79 ± 0.04	7.76 ± 0.07	-0.03 ± 0.11
R760 ref.	500-1000 V	7.85 ± 0.05	7.92 ± 0.06	0.07 ± 0.11
R2496 irr.	500-1500 V	6.11 ± 0.05	6.44 ± 0.05	0.33 ± 0.10
R2496 irr.	500-1000 V	6.23 ± 0.04	6.51 ± 0.06	0.28 ± 0.10
R2496 ref.	500-1500 V	5.75 ± 0.04	5.70 ± 0.07	-0.05 ± 0.11
R2469 ref.	500-1000 V	5.71 ± 0.03	5.84 ± 0.04	0.13 ± 0.07

Table 4.4: Relative gain before and after irradiation of all PMTs. The systematic error was introduced to take into account differences in the fitted values of α from HV scans performed by lowering/rising the HV.

4.2.4 Absolute gain

A possible approach to measure the absolute gain of a PMT is to measure the anodic charge produced when only one electron is emitted by the photocathode. With this method, the absolute gain of a PMT can be computed as:

$$G = \frac{Q_{anode}}{Q_e} \tag{4.3}$$

where Q_{anode} is the charge produced by the PMT in response to a single photoelectron, and Q_e is the electron charge.

As mentioned in Sect. 4.1, these measurements were made using an LED as light source, fed by a square-signal pulse of variable amplitude and duration of 20 ns. The PMTs supply voltage was set large enough to see the signal originated by a single photoelectron.
The single photoelectron condition was checked with an oscilloscope before taking charge measurements by enabling the screen persistency and triggering on the pulse provided to the LED: both a baseline (no emission of photoelectrons from the PMT photocatode) and some signals have ho be visible (the probability to emit an electron for the photocatode is < 1). An example of single photoelectron (pe) charge spectrum can be observed in Fig. 4.10: The first peak represents the pedestal (integrated over the signal baseline), when no photoelectron are actually emitted by the photocatode. The second one corresponds to the presence of just one photoelectron.

The charge distribution is fitted with the following function:

$$S(x) = G_{bk}(Q_0, \sigma_0) + \sum_{n=0}^{+\infty} \frac{e^{-\mu}}{n!} \mu^n \cdot G(Q_n, \sigma_n) \tag{4.4}$$

where $G_{bk}(Q_0, \sigma_0)$ is a gaussian function that describes the pedestal and the summation represents a poissonian function that describes the probability of having n photoelectrons if the expected mean value is μ, weighted by another gaussian function that describes the resolution of the charge distribution of events with n photoelectrons.
The single pe charge, which is represented by the parameter Q_1 in eq. (4.4),

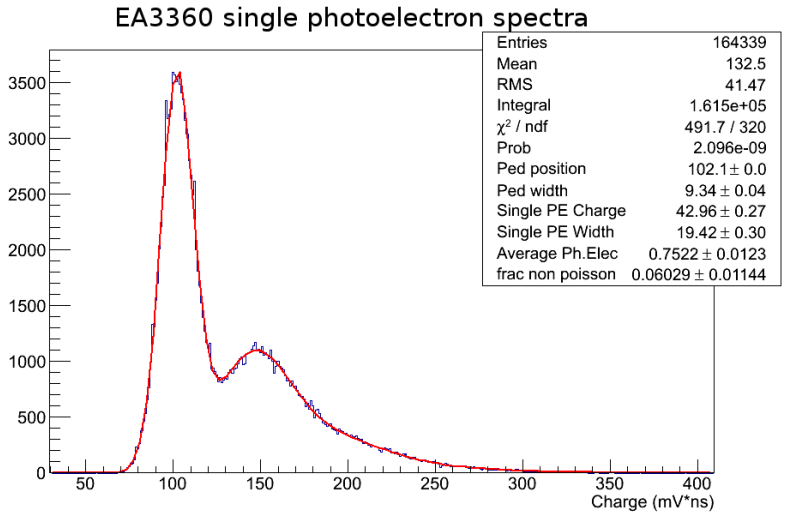

Figure 4.10: Single photoelectron spectrum for PMT EA3360 at 1240 V of supply voltage. Two peaks corresponding to zero (near to 100 mv*ns) and one (near 150 mv*ns) photoelectron emission are discernible.

is converted from mV · ns to picoCoulomb by dividing it by the impedance of the FADC channel (50Ω). The absolute gain is then computed using eq.(4.3). Table 4.5 shows the absolute gain with its statistical error computed for all PMTs before and after neutron irradiation of those under test.

PMT	**HV**	**G (before irrad.)**	**G (after irrad.)**	**ΔG**
R760 irr.	1200 V	$(5.39 \pm 0.04) \cdot 10^6$	$(4.66 \pm 0.08) \cdot 10^6$	$(-0.73 \pm 0.12) \cdot 10^6$
R760 ref.	1200 V	$(3.40 \pm 0.05) \cdot 10^6$	$(2.83 \pm 0.10) \cdot 10^6$	$(-0.57 \pm 0.15) \cdot 10^6$
R2496 irr.	1400 V	$(8.91 \pm 0.05) \cdot 10^6$	$(8.83 \pm 0.12) \cdot 10^6$	$(-0.08 \pm 0.17) \cdot 10^6$
R2496 ref.	1400 V	$(6.13 \pm 0.05) \cdot 10^6$	$(6.25 \pm 0.05) \cdot 10^6$	$(-0.12 \pm 0.10) \cdot 10^6$

Table 4.5: Absolute gain of all PMTs at a chosen supply voltage.

The measurements of the absolute gain of model 2496 PMTs taken before and after irradiation are consistent within the statistical errors. For model

R760, a gain decrease is apparent from the measurements. However, this effect is present in both the irradiated and the reference PMT at similar levels, and we consider it as a systematics rather than a real effect of neutron irradiation.

Chapter 5

Conclusion

The LHC just restarted after a shutdown phase for upgrades, with doubled beam energy and expected increasing luminosity over the next three years.
These upgrades in the accelerator required major upgrades of the ATLAS detectors as well, in order to maintain and eventually increase the performance of Phase I under the new operating conditions.
As far as the LUCID luminosity monitor is concerned, it was mandatory to reduce the photomultipliers (PMT) occupancy, which was obtained by reducing the geometric acceptance of its PMTs. Two possible substitute models with a smaller window size were taken into consideration during the shutdown: Hamamatsu R760 and R2496. In order to decide which PMT model is more suitable to be employed in LUCID, it was necessary to test their resistance to radiation first.
For this purpose, a PMT per model was irradiated in the Laboratories of Casaccia, first with gamma rays, and then with neutrons. Both with the expected doses for Phase II: $2 \cdot 10^5$ Gy for gamma rays and a fluence of $2.7 \cdot 10^{14}$ neutrons/cm^2.
During the work for this thesis the candidate participated to the measurements of the main PMTs characteristics (dark current, spectral response, relative and absolute gain) after neutron irradiation, and analysed the re-

sults.

Similarly to that observed after gamma ray irradiation, only a Dark Current increase, of about one order of magnitude after three weeks, was observed. Except for this, the spectral response, absolute and relative gain of the PMT under test did not present variations in excess of the precision of the measurements performed. Therefore, both PMT were considered suitable for LUCID phase II as far as radiation resistance is concerned. The final choice was in fact based on different criteria, like the effect of the window shape on the PMT signal distribution, and the overall ageing as a function of produced current.

LUCID is currently providing the official luminosity measurement of LHC in the ATLAS interaction point, both for online monitoring and offline measurement of process cross sections.

Bibliography

[1] http://home.web.cern.ch/topics/large-hadron-collider

[2] ATLAS Collaboration, The ATLAS Experiment at the CERN Large Hadron Collider, JINST 3 (2008) S08003

[3] ATLAS Collaboration, ATLAS Forward Detectors for Measurement of Elastic Scattering and Luminosity

[4] ATLAS Collaboration, Improved luminosity determination in pp collisions at s = 7 TeV using the ATLAS detector at the LHC

[5] William R. Leo, Techniques for Nuclear and Particle Physics Experiments: A How-To Approach
Springer-Verlag

[6] Hamamatsu: Photomultiplier Tubes - Basics and Application
Hamamatsu Photonics K.K.,2006.

[7] https://www.hamamatsu.com/us/en/R760.html
https://www.hamamatsu.com/us/en/R2496.html

[8] John R. Taylor, Introduzione all'analisi degli errori
Zanichelli, 2000

Ringraziamenti

Il mio primo ringraziamento va alla mia correlatrice, la Dottoressa Carla Sbarra, che mi ha assistito nell'intero lavoro di tesi. La ringrazio per la sua estrema disponibilità e pazienza, per il tempo e l'attenzione dedicatami, e per la precisione con cui ha più volte revisionato questa tesi.
Ringrazio il mio relatore, il Professor Nicola Semprini-Cesari, per avermi dato la possibilità di fare questa tesi e per la disponibilità dimostratami.
Ringrazio infine i miei genitori, per tutto il supporto dimostratomi in questi anni.